Shock Tube and Modeling Study of Methylamine Thermal Decomposition

T. Higashihara, W. C. Gardiner, Jr.,* and S. M. Hwang

Department of Chemistry, University of Texas, Austin, Texas 78712 *(Received: September 9, 1986)*

The thermal decomposition of CH_3NH_2 was studied by IR laser kinetic absorption spectroscopy behind reflected shock waves with $1400 < T_5 < 1820$ K and $4.0 \times 10^{-6} < \rho_5 < 8.0 \times 10^{-6}$ mol cm^{-3}. The absorption profiles were satisfactorily modeled with a 28-reaction mechanism based on earlier investigations. The initial decomposition was found to be dominated by $CH_3NH_2 + M \rightarrow CH_3 + NH_2 + M$ ($\Delta H°_0 = 350$ kJ) under these conditions, for which the rate constant expression $k_1 = 5 \times 10^{17} \exp(-260 \text{ kJ}/RT)$ cm^3 mol^{-1} s^{-1} was derived.

Introduction

Nitrogen-containing compounds present in fuels contribute part of the NO_x emissions from practical combustion devices. It is generally thought that these compounds are rapidly converted to HCN and NH_3 in flames and that "fuel NO_x" chemistry consists of the subsequent reactions of these species. In order to derive a picture of the underlying kinetics governing the generation of HCN and NH_3 from fuel nitrogen, we investigated the pyrolytic decomposition of CH_3NH_2 in shock waves as a model fuel nitrogen decomposition process. The experimental study was supported by computer modeling using a reaction mechanism based upon earlier research on CH_3NH_2 and its decomposition products.

There is a substantial older literature on CH_3NH_2 kinetics. Emeleus and Jolley[1,2] studied the thermal decomposition reaction in a static reactor over the temperature range $833 < T < 952$ K and found the product distribution to be $H_2/HCN/CH_4/NH_3 = 10/5/1/1$. The decomposition rate was first-order in CH_3NH_2 with a rate constant expression $3.4 \times 10^{11} \exp(-58 \text{ kcal}/RT)$ s^{-1} for $CH_3NH_2 \rightarrow HCN + 2H_2$. They suggested that the decomposition is a chain reaction based on methylimine radicals:

$$CH_3NH_2 \rightarrow CH_3 + NH_2$$

$$CH_3 + CH_3NH_2 \rightarrow CH_4 + CH_3NH \rightarrow CH_4 + CH_2NH + H$$

$$NH_2 + CH_3NH_2 \rightarrow NH_3 + CH_3NH \rightarrow NH_3 + CH_2NH + H$$

$$H + CH_3NH_2 \rightarrow H_2 + CH_3NH \rightarrow H_2 + CH_2NH + H$$

$$CH_2NH \rightarrow HCN + H_2$$

Johnson and Lovas[3] pyrolyzed CH_3NH_2 in a flow tube and recorded the microwave spectrum of CH_2NH. Peel and Willett[4] pyrolyzed CH_3NH_2 in a flow tube at 1228 and 1543 K and recorded photoelectron spectra. At 1228 K, HCN, H_2, and about 5% CH_2NH were detected, while at 1543 K a small amount of NH_3 as well as HCN and H_2 were detected, but not CH_2NH. Evans et al.[5] studied CH_3NH_2 multiphoton dissociation and measured yields of CH_4, H_2, and C_2H_6 using gas buret mass spectroscopy. The product distribution was found to depend on pressure, fluence, and pulse width; generally, the H_2 yield was much larger (>10:1) than that of CH_4 and the C_2H_6 yield was less than 20% of the CH_4 yield. These studies together show that for the conditions investigated the main products of CH_3NH_2 decomposition are H_2 and HCN and that CH_2NH is present as a relatively stable intermediate species.

The thermal decomposition of CH_3NH_2 in shock waves was studied by Dorko et al.[6] using infrared thermal emission at wavelengths of band systems of CH_3NH_2 and NH_3 over the temperature range $1275 < T < 2400$ K and the pressure range $1 < P < 10$ atm. They observed first-order decay at the first wavelength and first-order production at the second, with the production rate constant being about half of the decay rate constant. They proposed the decomposition mechanism

$$CH_3NH_2 \rightarrow CH_3 + NH_2$$

$$CH_3 + CH_3NH_2 \rightarrow CH_4 + CH_2NH_2$$

$$CH_3 + CH_2NH_2 \rightarrow CH_4 + CH_2NH$$

$$NH_2 + CH_3NH_2 \rightarrow NH_3 + CH_2NH_2$$

$$NH_2 + CH_2NH_2 \rightarrow NH_3 + CH_2NH$$

$$CH_2NH \rightarrow H_2 + HCN$$

According to this mechanism, 2 mol of CH_3NH_2 would give 1 mol each of H_2, HCN, CH_4, and NH_3, quite different from the distribution found in the static reactor and flow tube studies.

The reaction mechanism of CH_3NH_2 thermal decomposition has clearly not been established by the investigations reported so far. Moreover, there is only a limited amount of information on the rate constants of the elementary reactions expected to participate. We undertook to measure the thermal decomposition rate in shock waves by IR laser kinetic absorption spectroscopy and to subject the new and old data to a detailed computer modeling study.

Experimental Section

The apparatus and techniques used have been described in detail elsewhere.[7] A 2948-cm^{-1} He-Ne laser beam was passed through a 9.6-cm-wide rectangular shock tube; a 1.5-mm exit slit and an interference filter 20 cm from the exit slit removed all thermal emission up to the highest temperatures of the experiments. The InSb detector signal was recorded at 10-bit, 20-MHz resolution by a Hewlett-Packard 5180A waveform recorder controlled by a Hewlett-Packard 9236 computer.

CH_3NH_2 was synthesized by dropping saturated CH_3NH_3Cl (99+% stated purity) solution onto KOH or NaOH pellets under a nitrogen atmosphere and dried by passage through two $CaCl_2$ U-tubes before condensation in an acetone-dry ice trap. The product was distilled 4-8 times under vacuum before being used for test gas preparation. Test gas mixtures were prepared manometrically and stored for at least 48 h before use in 24-dm^3 glass bulbs.

The test gas compositions used were 2.5% and 5% CH_3NH_2 in Ar. Starting pressures were 20 Torr for the 2.5% mixture and 10 and 20 Torr for the 5% mixture, giving reflected shock densities in the range $(4.0-8.0) \times 10^{-6}$ mol cm^{-3} over the temperature range 1400-1820 K.

The experimental results were interpreted with the aid of computer modeling using the assumption of constant-density

(1) Jolley, L. J. *J. Chem. Soc.* **1934**, 1957.
(2) Emeleus, H. J.; Jolley, L. J. *J. Chem. Soc.* **1935**, 929.
(3) Johnson, D. R.; Lovas, F. J. *Chem. Phys. Lett.* **1972**, *57*, 65.
(4) Peel, J. B.; Willett, G. D. *J. Chem. Soc., Faraday Trans. 2* **1975**, *71*, 1799.
(5) Evans, D. K.; McAlpine, R. D.; Adams, H. M.; Creagh, A. L. *Chem. Phys.* **1983**, *80*, 379.
(6) Dorko, E. A.; Pchelkin, N. R.; Wert, J. C., III; Mueller, G. W. *J. Chem. Phys.* **1979**, *83*, 297.
(7) Olson, D. B.; Tanzawa, T.; Gardiner, W. C., Jr. *Int. J. Chem. Kinet.* **1979**, *11*, 23.

0022-3654/87/2091-1900$01.50/0

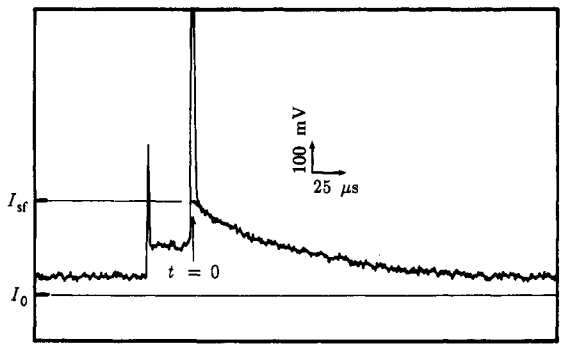

Figure 1. Sample experimental record of transmitted laser intensity. Full intensity I_0 = 6680 mV. Time zero was taken from the center of the reflected shock schlieren spike. Test gas 2.5% CH_3NH_2, 97.5% Ar, P_1 = 20 Torr, T_5 = 1600 K. The indicated extrapolation of the reflected shock signal intensity was used to obtain the shock-front transmitted intensity I_{sf} for kinetic analysis and to derive an extinction coefficient data point.

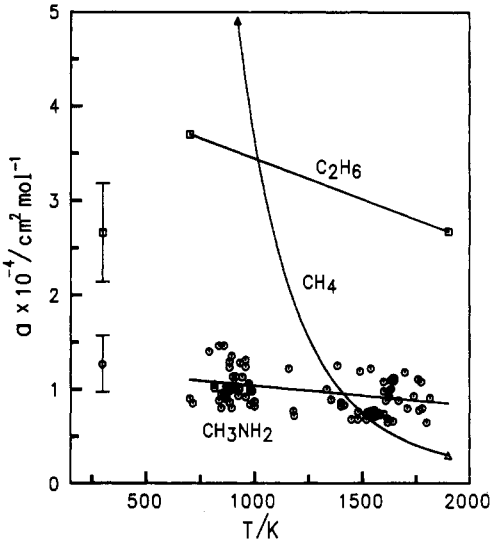

Figure 2. Decadic absorptivity for CH_3NH_2 compared to that of methane (□, ref 10) and ethane (△, ref 7). CH_3NH_2 data (○) at temperatures below 1000 K are from incident shock waves.

reaction under the reflected shock conditions computed from the incident shock speed under the assumption of complete vibrational relaxation but no chemical reaction in both incident and reflected waves.[8] For species whose standard thermochemical properties are not available,[9] rigid-rotor, harmonic oscillator formulas were used to compute the thermochemical properties; see footnotes to Table I.

Results

A representative laser absorption profile is shown in Figure 1. In order to obtain the shock-front absorbance values, the profiles were extrapolated to the center of the 4-μs-wide schlieren spikes. The decadic molar absorptivities of CH_3NH_2 derived from incident wave absorbances and extrapolated reflected shock-front absorbances are shown in Figure 2 together with those of C_2H_6[7] and CH_4.[10] The least-squares fit to the high-temperature data gives for CH_3NH_2 the expression a/cm^2 mol^{-1} = $1.25 \times 10^4 - 2.09T$. It can be seen that the room-temperature absorptivity is close to half of that of C_2H_6 (CH_3NH_2 having half of the C–H stretches of C_2H_6), while at high temperatures the two absorptivities are further apart.

(8) Gardiner, W. C., Jr.; Walker, B. F.; Wakefield, C. B. In *Shock Waves in Chemistry*; Lifshitz, A., Ed.; Marcel Dekker: New York, 1981; p 319.
(9) Burcat, A. In *Combustion Chemistry*; Gardiner, W. C., Jr., Ed.; Springer-Verlag: New York, 1984; p 455.
(10) Simmie, J. M.; Gardiner, W. C., Jr.; Eubank, C. S. *J. Phys. Chem.* **1982**, *86*, 799.

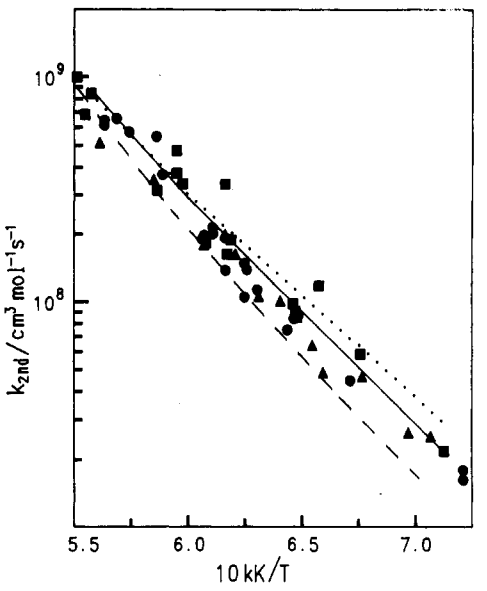

Figure 3. Arrhenius presentation of early time rates expressed as $k_{2nd} = \ln (1/0.9)/(t_{90}[M]_5)$ (see text): (● and ---) 2.5% CH_3NH_2, 97.5% Ar, P_1 = 20 Torr; (■ and ···) 5% CH_3NH_2, 95% Ar, P_1 = 10 Torr; (▲ and —) 5% CH_3NH_2, 95% Ar, P_1 = 20 Torr. The lines are modeling results using the Table I rate constants.

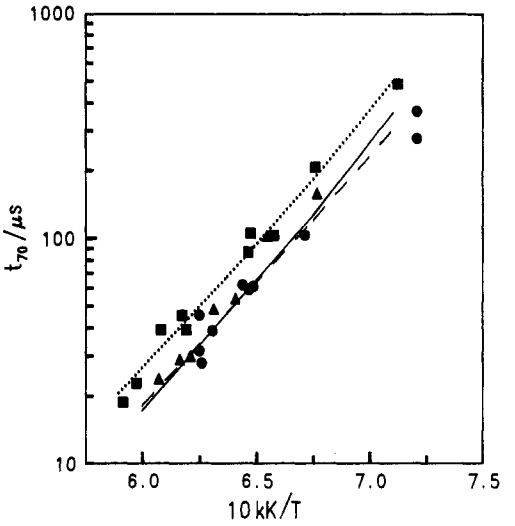

Figure 4. Arrhenius presentation of later time rates, expressed as times for absorbed intensity to fall to 70% of reflected shock-front value. Symbols and lines as in Figure 3.

Reaction progress was characterized by measuring the times t_{90} and t_{70} required for decrease of the absorbed intensity to 90% and 70% of the reflected shock-front values. The t_{90} values proved in the modeling analysis (vide infra) to be attributable almost entirely to loss of CH_3NH_2 absorption, while the contributions from C_2H_6 and CH_4 to the t_{70} values were computed to be appreciable. The t_{90} data were converted to the form of second-order rate constants through the reflected shock density $[M]_5$ and the definition

$$k_{2nd} = \ln (1/0.9)/(t_{90}[M]_5) \text{ cm}^3 \text{ mol}^{-1} \text{ s}^{-1}$$

In the early part of the reaction k_{2nd} is close to the second-order disappearance rate constant of CH_3NH_2. In the center of the temperature range studied the scatter of the k_{2nd} data is about ±25%, most of which stems from the uncertain extrapolation to the shock-front transmitted intensity values. It is seen in Figure 3 that the second-order treatment condenses the three sets of data together. The lines are modeling results discussed later.

An Arrhenius presentation of the t_{70} data is given in Figure 4. It can be seen that the two sets of data for P_1 = 20 Torr fall together, while the P_1 = 10 Torr data show distinctly longer times.

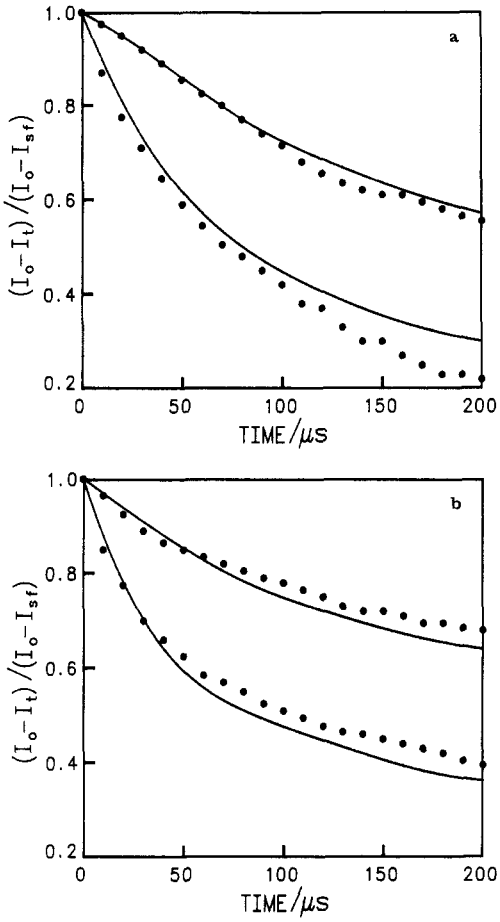

Figure 5. Absorption decrease profiles: (a) 2.5% CH_3NH2, P_1 = 20 Torr, and T_5 = 1490 K (upper) and 1600 K (lower); (b) 5% CH_3NH_2, P_1 = 20 Torr, T_5 = 1480 K (upper) and 1610 (lower); (●) experimental profiles, (—) modeling results using the Table I rate constants.

The lines show modeling results discussed later.

The reaction mechanism adopted for computer modeling is shown in Table I.[11-15] It includes the two sets of reactions discussed above and was expanded to include the elementary reactions of C_2H_6, CH_4, and NH_3 thermal decomposition. The enthalpies of reaction at 0 K were derived from the BAC-MP4 thermochemistry of Melius and Binkley.[11]

The initiation reaction 1 is expected to dominate the chain initiation process on thermochemical grounds, the bond strength of the C–N bond 350 kJ being substantially less than the bond strengths of the C–H and N–H bonds, 384 and 422 kJ, respectively. The NH_2 radical was indeed detected by LIF in the multiphoton dissociation study of CH_3NH_2 by Filseth et al.[12]

It was assumed that abstraction reactions from CH_3NH_2 would remove the C hydrogens only. This is supported by the greater bond strength of the N–H bond (38 kJ stronger according to the BAC-MP4 thermochemistry, from 33 to 60 kJ stronger according to other evaluations[13-15]) and the 3:2 ratio of C and N hydrogens. There is, however, evidence from low-temperature (388–488 K) studies[16] that abstraction of the N hydrogens also occurs. At 1600 K the rate constant expressions of Gray and Thynne[16] suggest a ratio of C–H to N–H abstraction of about 10. It will be seen later that addition of N–H abstraction reactions would not change the predicted course of the decomposition process.

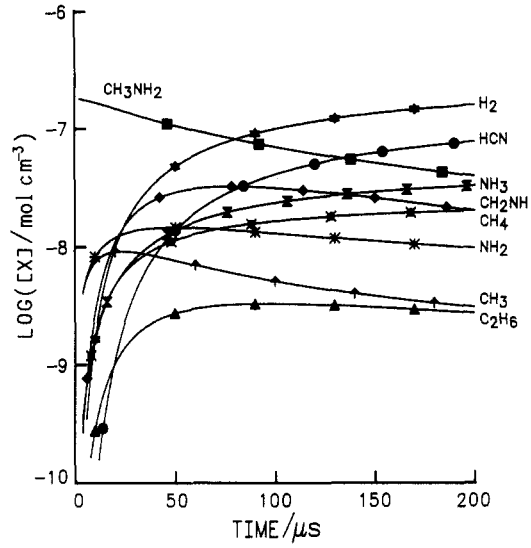

Figure 6. Computed concentration profiles for 2.5% CH_3NH_2, P_1 = 20 Torr, T_5 = 1570 K.

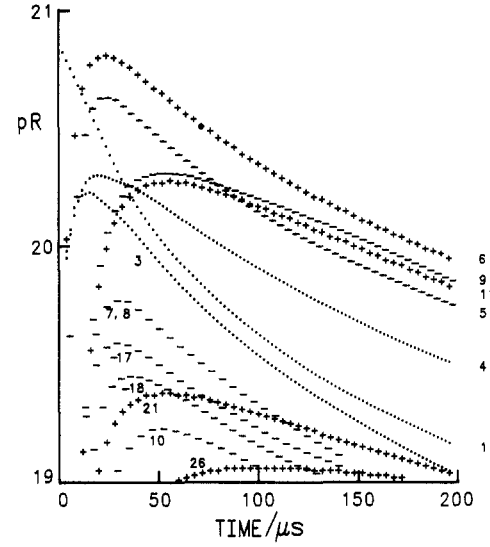

Figure 7. Reaction rate (pR) profiles for computation of Figure 6: (···) reactions consuming CH_3NH_2; (+++) reactions producing H atoms; (---) reactions consuming H atoms. Reactions with maximum rates less than 4% of the maximum rate of the fastest reaction in each class are not shown.

Reactions of NH, CH_2, and CH radicals were assumed to be minor processes that might occur only in the latest stages of the high-temperature reaction without affecting the course of CH_3NH_2 decomposition itself.

Except for the methyl abstraction reaction 3, rate constant expressions for the elementary reactions of CH_3NH_2, CH_2NH_2, CH_2NH, and CHNH have not been reported. For modeling purposes these rate constants were assigned as follows. The rate constant of the initiation reaction 1 was set equal to the least-squares fit to the k_{2nd} data between 1480 and 1700 K. The rest were assumed to have the same values as the analogous reactions of corresponding C_2 species. Rate constants for reactions 1 through 12 were then varied systematically until satisfactory fits to the k_{2nd} and t_{70} data (Figures 3 and 4) were obtained. The final expressions are given in Table I. It can be seen in Figure 5 that not only the k_{2nd} and t_{70} data but also the entire profiles are well reproduced by the Table I mechanism and rate constant expressions.

In Figure 6 the computed species concentration profiles are shown for 2.5% CH_3NH_2 test gas at 1570 K. From these profiles it is found that CH_4 and C_2H_6 contribute only 3% of the total absorbance at t_{90} and 20% at t_{70}, supporting the starting assumption that the k_{2nd} values reflect CH_3NH_2 decomposition

(11) Melius, C. F.; Binkley, J. S. *Symp. (Int.) Combust., [Proc.], 21st*, in press.
(12) Filseth, S. V.; Danon, J.; Feldman, D.; Campbell, I. D.; Welge, K. H. *Chem. Phys. Lett.* **1979**, *63*, 615.
(13) Golden, D. M.; Solly, R. K.; Gac, N. A.; Benson, S. W. *J. Am. Chem. Soc.* **1972**, *94*, 363.
(14) Colussi, A. J.; Benson, S. W. *Int. J. Chem. Kinet.* **1977**, *9*, 307.
(15) Grela, M. A.; Colussi, A. J. *J. Phys. Chem.* **1984**, *88*, 595.
(16) Gray, P.; Thynne, J. C. J. *Trans. Faraday Soc.* **1963**, *59*, 2275.

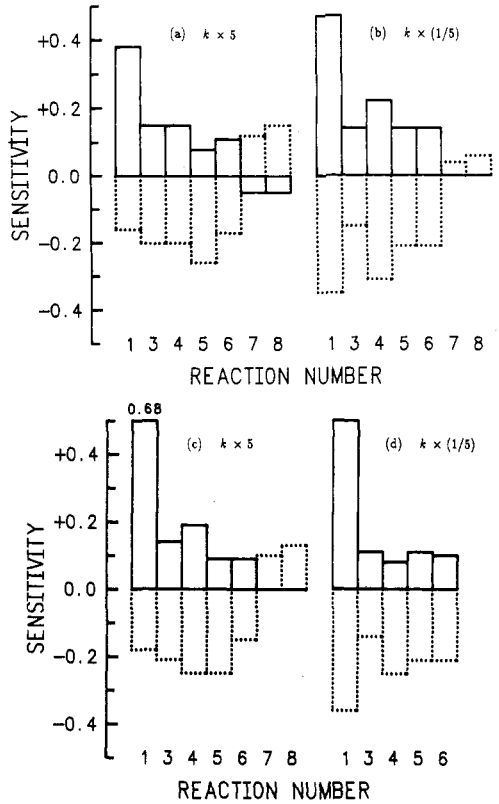

Figure 8. Logarithmic response sensitivity spectra (ref 17) for k_{2nd} (solid boxes) and t_{70} (dotted boxes) computed for 5% (a and b) and 2.5% (c and d) mixtures with P_1 = 20 Torr and T_5 = 1570 K. Spectra a and c were computed by multiplying Table I rate constant values by 5, and spectra b and d were computed by multiplications by $^1/_5$. Sensitivity values less than 0.03 are not shown.

directly. It is also seen that the predicted product distribution at long reaction times, $H_2/HCN/NH_3/CH_4/CH_2NH$ = 10/5/2/1/1, is close to the low-temperature results of Jolley[1] and Peel and Willett.[4]

In order to display the reaction fluxes, we computed the pR values[17] (logarithms of absolute values of net reaction rates in molecules cm^{-3} s^{-1} units prefaced with negative signs to denote prevalence of reverse reaction) as functions of reaction time (Figure 7). It is seen that for these conditions the unimolecular reaction dominates the first 10 μs of reaction, while at later time CH_3NH_2 decomposes by the H atom chain of reactions 5 and 6. At higher temperatures reaction 1 contributes more, and at lower temperatures less.

Sensitivity spectra for k_{2nd} and t_{70} determined by multiplications and divisions by 5 are shown in Figure 8. It is seen that reaction 1 is substantially more important than the other main chain reactions in determining k_{2nd}, that the whole set of main chain reactions combines to determine t_{70}, and that the secondary reactions 9–28 are unimportant as far as the absorption profiles are concerned.

Modeling was also undertaken for interpretation of the results reported by Dorko et al.[6] Attention was concentrated on three aspects of their results: (1) The IR emissions attributed to both CH_3NH_2 and NH_3 show first-order kinetics. (2) The reaction order with respect to CH_3NH_2 varies from 0.32 at the highest pressures studied to 0.78 at the lowest pressures. (3) The absolute rate of CH_3NH_2 decomposition is about twice the rate of NH_3 appearance.

Experimental and computed profiles for the sample case given by Dorko et al.[6] are shown in Figure 9. It became clear in the course of modeling for these conditions that the rate of NH_3 production was sensitive to the rate constant for reaction 4 and that matching their experimental profiles could be accomplished

(17) Gardiner, W. C., Jr. *J. Phys. Chem.* **1977**, *81*, 2367.

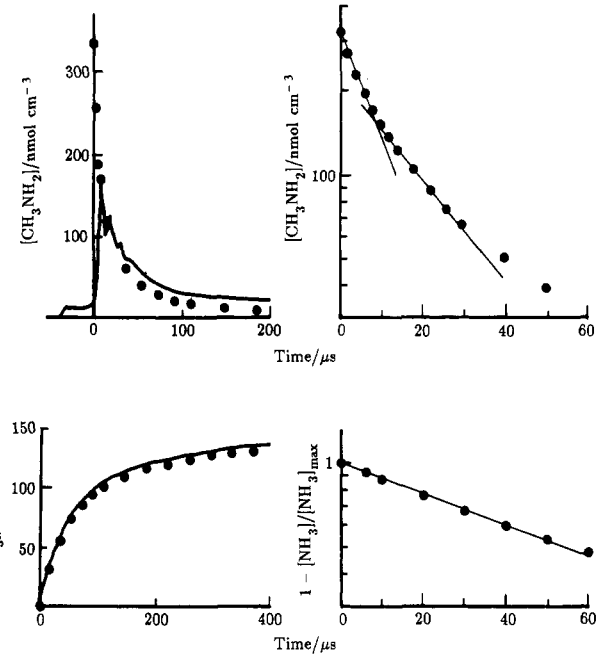

Figure 9. Comparison of experimental results from ref 6 with profiles computed using the Table I reaction mechanism and rate constants. The lines are from Figures 1 and 2 of ref 6; the points denote computed results for an experiment using 1% CH_3NH_2 test gas with T_5 = 1678 K, ρ_5 = 3.32 × 10^{-5} mol cm^{-3} (3.375-μm emission, upper traces) and T_5 = 1635 K, ρ_5 = 3.29 × 10^{-5} mol cm^{-3} (2.886-μm emission, lower traces). The computed results were scaled to the experimental traces for the 3.375-μm emission by matching the first peak of the trace and assuming that CH_3NH_2 was the only emitter. See ref 6 for procedure used to scale 2.886-μm emission according to an estimated long time asymptote; the computed NH_3 profile was scaled in an analogous manner.

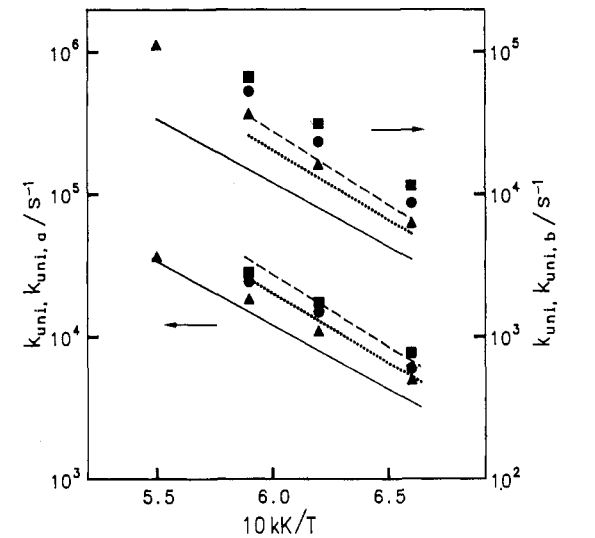

Figure 10. Unimolecular rate constants derived from early ($k_{uni,b}$) and late ($k_{uni,a}$) exponential decay rates computed by modeling 1% CH_3NH_2 thermal dissociation with the Table I mechanism and rate constants at densities of 2.75 × 10^{-5} mol cm^{-3} (▲ and —), 5.3 × 10^{-5} mol cm^{-3}, (● and ···), and 8.37 × 10^{-5} mol cm^{-3} (■ and – – –). The lines indicate the experimental results (k_{uni}) of ref 6.

by dividing the Table I expression by 2. In the semilogarithmic presentation (Figure 9, upper right) is seen that the computed profiles for these conditions have quite different slopes—by about a factor of 2—before and after about 10 μs. The corresponding rate constants $k_{uni,b}$ and $k_{uni,a}$ are shown in Figure 10 together with the k_{uni} expression derived from the data by Dorko et al. The experimental expression clearly corresponds to the $k_{uni,a}$ rate, as expected from the time constant of the apparatus evident in the experimental trace. It was found that $k_{uni,a}$ was sensitive to k_3, k_4, and k_5 but not to k_6. One can see from Figure 10 that the

TABLE I: Reaction Mechanism, Rate Constant Expressions, and Rate Constants at 1570 K[a]

reaction	$\Delta H°_0$	A	m	E_A	k_f	k_r	ref
1. $CH_3NH_2 + M \rightarrow CH_3 + NH_2 + M$	350	4.8×10^{17}		262	9.2×10^{8}	1.3×10^{17}	this work
2. $CH_3NH_2 + M \rightarrow CH_2NH_2 + H + M$	384	2.0×10^{17}		370	9.6×10^{4}	4.0×10^{15}	$= k_{17}$
3. $CH_3 + CH_3NH_2 \rightarrow CH_4 + CH_2NH_2$	−46	0.55	4	35	2.3×10^{11}	2.7×10^{9}	$= k_{22}$
4. $NH_2 + CH_3NH_2 \rightarrow NH_3 + CH_2NH_2$	−67	1.3×10^{14}		84	2.1×10^{11}	1.3×10^{9}	adjusted
5. $H + CH_3NH_2 \rightarrow H_2 + CH_2NH_2$	−62	5.5×10^{12}		13	2.1×10^{12}	1.0×10^{9}	adjusted
6. $CH_2NH_2 \rightarrow H + CH_2NH$	155	1.5×10^{11}		167	4.0×10^{5}	7.7×10^{11}	adjusted
7. $H + CH_2NH_2 \rightarrow H_2 + CH_2NH$	−277	1.0×10^{13}		0	1.0×10^{13}	2.2×10^{5}	adjusted
8. $H + CH_2NH_2 \rightarrow CH_3 + NH_2$	−34	1.0×10^{13}		0	1.0×10^{13}	3.5×10^{10}	adjusted
9. $H + CH_2NH \rightarrow H_2 + CHNH$	−41	1.5×10^{14}		42	6.1×10^{12}	3.9×10^{9}	$= k_{25}$
10. $H + CHNH \rightarrow H_2 + HCN$	−356	2.0×10^{13}		0	2.0×10^{13}	2.0×10^{3}	$= k_{27}$
11. $CHNH + M \rightarrow H + HCN + M$	76	3.0×10^{15}		134	1.0×10^{11}	8.7×10^{13}	$= k_{26}$
12. $CH_2NH + M \rightarrow H_2 + HCN + M$	36	1.0×10^{9}		0	1.0×10^{9}	5.3×10^{8}	see text
13. $H_2 + CN \rightarrow H + HCN$	−66	7.5×10^{13}		0	7.5×10^{13}	7.3×10^{11}	*b*
14. $NH_3 + M \rightarrow NH_2 + H + M$	451	2.5×10^{16}		392	2.2×10^{3}	1.4×10^{16}	*c*
15. $NH_3 + H \rightarrow NH_2 + H_2$	19	1.3×10^{14}		90	1.3×10^{11}	1.0×10^{10}	*c*
16. $N_2H_4 + M \rightarrow NH_2 + NH_2 + M$	282	4.0×10^{15}		172	8.0×10^{9}	1.4×10^{15}	*d*
17. $CH_4 + M \rightarrow CH_3 + H + M$	430	2.0×10^{17}		370	9.6×10^{4}	3.4×10^{17}	*e*
18. $CH_3 + H_2 \rightarrow CH_4 + H$	2	6.5×10^{2}	3	32	2.1×10^{11}	5.2×10^{12}	*e*
19. $C_2H_6 + M \rightarrow CH_3 + CH_3 + M$	362	6.3×10^{19}		345	2.1×10^{8}	1.6×10^{17}	7
20. $C_2H_6 + H \rightarrow C_2H_5 + H_2$	201	1.3×10^{14}		39	6.4×10^{12}	4.2×10^{10}	*f*
21. $C_2H_5 + M \rightarrow C_2H_4 + H + M$	146	1.0×10^{17}		146	1.3×10^{12}	1.5×10^{18}	*g*
22. $C_2H_6 + CH_3 \rightarrow C_2H_5 + CH_4$	−13	0.55	4	35	2.3×10^{11}	3.8×10^{10}	*e*
23. $H + C_2H_5 \rightarrow CH_3 + CH_3$	−55	3.0×10^{13}		0	3.0×10^{13}	4.0×10^{10}	*e*
24. $H + C_2H_5 \rightarrow C_2H_4 + H_2$	−286	1.7×10^{12}		0	1.7×10^{12}	2.2×10^{4}	*f*
25. $H + C_2H_4 \rightarrow H_2 + C_2H_3$	−16	1.5×10^{14}		43	5.7×10^{13}	3.5×10^{11}	*e*
26. $C_2H_3 + M \rightarrow C_2H_2 + H + M$	148	3.0×10^{15}		134	1.0×10^{11}	2.9×10^{16}	*e*
27. $H + C_2H_3 \rightarrow H_2 + C_2H_2$	−284	2.0×10^{13}		0	2.0×10^{13}	6.5×10^{4}	*e*
28. $CH_3 + CH_3 \rightarrow C_2H_4 + H_2$	−231	1.0×10^{16}		134	3.5×10^{11}	3.4×10^{5}	*e*

[a] Units are mol cm^{-3}, s, and kJ. Rate constants were expressed as $k = AT^m \exp(-E_A/RT)$. Those for reactions footnoted "adjusted" were modified from the starting expressions so as to optimize the fit to experimental data. Because of the coupling between the members of the H-stripping chain, other combinations of rate constant expressions for these reactions would provide equally good fits to the data. Reverse reactions were automatically included in the computer program through equilibrium constants computed from polynomial fits to standard thermochemical data. The basic thermochemical data source was the 1971 JANAF table (Stull, D. R.; Prophet, H. *JANAF Thermochemical Tables*, 2nd ed.; U.S. National Bureau of Standards: Washington, DC, 1971; NSRDS-NBS 37) with the following additions. The properties of CH_3NH_2, C_2H_6, and C_2H_5 were derived from rigid-rotor, harmonic oscillator calculations; the results were identical with those given by Burcat.[9] For C_2H_3 the data of Duff and Bauer (Duff, R. E.; Bauer, S. H. *J. Chem. Phys.* **1962**, *36*, 1754) were used. For CH_2NH_2 a rigid-rotor, harmonic oscillator estimation was made using the remaining frequencies and the moments of inertia of CH_3NH_2; the standard enthalpy of formation was that given by Grela and Colussi.[15] For CH_2NH the thermodynamic properties of Jacox and Milligan (Jacox, M. E.; Milligan, D. E. *J. Mol. Spectrosc.* **1975**, *56*, 333) were combined with the standard enthalpy of formation given by DeFrees and Hehre (DeFrees, D. J.; Hehre, W. J. *J. Phys. Chem.* **1978**, *82*, 391). For CHNH the thermochemical properties were simply taken as those of C_2H_3; it was computed to decompose so quickly that its reverse reactions were always negligible. The standard enthalpies of reaction at 0 K are based on the BAC-MP4 thermochemistry of Melius and Binkley[11] and differ in minor respects from the values adopted for the simulations. [b] Szekely, A.; Hanson, R. K.; Bowman, C. T. *Int. J. Chem. Kinet.* **1983**, *15*, 915. [c] Hanson, R. K.; Salimian, S. In *Combustion Chemistry*; Gardiner, W. C., Jr., Ed.; Springer-Verlag: New York, 1984. [d] Meyer, E.; Olschewski, H. A.; Troe, J.; Wagner, H. Gg. *Symp. (Int.) Combust., [Proc.], 12th* **1969**, 345. [e] Warnatz, J. In *Combustion Chemistry*; Gardiner, W. C., Jr., Ed.; Springer-Verlag: New York, 1984. [f] Camilleri, P.; Marshall, R. M.; Purnell, J. H. *J. Chem. Soc., Faraday Trans. 1* **1974**, *70*, 1434. [g] Hidaka, Y.; Shiba, S.; Takuma, H.; Suga, M. *Int. J. Chem. Kinet.* **1985**, *17*, 441; adjusted to pressure range of present experiments.

Table I mechanism and rate constant expressions account for the experimentally observed variation of the order with respect to CH_3NH_2 concentration.

The computed NH_3 appearance profiles were converted to first-order plots following the procedure of Dorko et al. The NH_3 yield was sensitive to k_1, k_3, and k_6; the NH_3 appearance rate was found to be determined mainly by k_4, the influences of other rate constants being rather small. The computed and experimental profiles are seen in Figure 11 to be in satisfactory agreement.

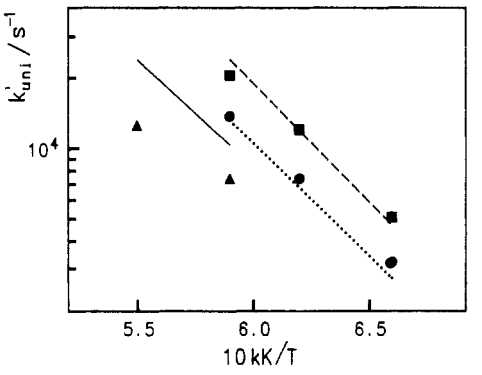

Figure 11. Unimolecular rate constant for appearance of NH_3. Symbols and lines as in Figure 10.

Discussion

Both the present IR absorption data and the IR thermal emission data of Dorko et al. were interpreted on the assumption that the absorbers and emitters are known. The rate constant expressions derived on this basis are readily shown to be lower bounds, valid for the case that absorptions or emissions from unappreciated reaction products do not contribute at all. Based upon the modeling results, there are indeed no such compensating absorptions for the IR laser absorption experiments.

The sensitivity spectra (Figure 8) show that the rate constant expressions derived in the modeling investigation give close accounting for the experimental profiles as a set but that other sets would give comparably good accounting for the data. We did not explore the possibility that the H-elimination reaction 6 could also have a molecular elimination channel. We did explore the likely possibility that reaction 12 is an atomic rather than a molecular elimination process, using the experimental rate constant expression for the analogous reaction of formaldehyde. While the intermediate concentrations were affected, the predicted decomposition profiles of CH_3NH_2 were not.

The analogy between the thermal decompositions of CH_3NH_2 and C_2H_6 is quite close. Both begin by scission of the bond connecting the heavy atoms; the products of this decomposition mostly abstract an H atom from the parent molecule, leaving a radical that quickly decomposes unimolecularly to form a relatively stable intermediate (C_2H_4 or CH_2NH) and an H atom; the rest of the reaction is predominantly attack of H atoms on the parent

molecules and later the intermediates until the composition of the gas approaches a steady state of the stable molecules (H_2, C_2H_2, C_2H_4, HCN). Under laboratory pyrolysis conditions, the endothermicity of the reaction leads to a substantial temperature drop; in flame pyrolysis, the temperature profile would be governed by other processes.

The product distribution for CH_3NH_2 pyrolysis is a function of pressure. As described above, the high-pressure result of Dorko et al.—about half of the CH_3NH_2 forming NH_3—is well accounted for by the Table I mechanism and rate constants. To test its predictive ability at low pressure, we modeled the Peel and Willett[4] conditions (ignoring the probable participation of wall reactions) of P = 1.2 Torr and T = 1543 K. In 50-ms reaction time about 27% of the CH_3NH_2 had decomposed to give products in the ratio $H_2/HCN/CH_2NH/CH_4/NH_3$ = 25/9/9/1/1. Their photoelectron spectroscopic result showed H_2, HCN, and a small amount of NH_3.

Of reactions 1–12, the only one for which an experimental rate constant has been provided is reaction 3, for which Gray and Thynne[16] give $k_3 = 10^{11} \exp(-8700 \text{ cal}/RT)$ cm^3 mol^{-1} s^{-1}. At 1600 K the Table I expression gives a value 40 times larger than this expression. If the Gray and Thynne expression were used in modeling, reaction 3 would make no contribution to the decomposition process. While some of the difference would be normal Arrhenius graph curvature,[18] it appears more reasonable to adopt the Table I expression, based upon the analogy to reaction 22, for decomposition modeling at this time. Further refinement of the rate constant expressions should be readily possible if shock tube experiments would be undertaken to obtain the high-temperature product distributions: stable products by single-pulse experiments and the intermediates CH_3 and NH_2 by absorption spectroscopy.

(18) Zellner, R. In *Combustion Chemistry*; Gardiner, W. C., Jr., Ed.; Springer-Verlag: New York, 1984; p 135.

Conclusions

The high-temperature thermal decomposition of CH_3NH_2 is a combination of two processes: unimolecular scission of the C–N bond and H-atom-catalyzed stripping of four H atoms from the parent molecule to form HCN and H_2. The relative contributions of the two pathways depend upon pressure and temperature. Because the stripping process is a sequential one combining two abstraction reactions with two unimolecular decompositions, only its overall rate is determinable through measuring the overall decomposition rate; measurements of intermediate concentrations would be required for assignment of rate constant expressions to the actual elementary steps. The initiation reaction 1 is, for the conditions studied, a normal bond-scission unimolecular decay in the falloff region.

Acknowledgment. This research was supported by the Robert A. Welch Foundation. We acknowledge a helpful discussion with C. F. Melius. T.H. expresses appreciation for financial support of the Ministry of Education, Science, and Culture of Japan.

Registry No. CH_3NH_2, 74-89-5.

Radiolytic Oxidation of 1,2,4-Benzenetriol. An Application of Time-Resolved Resonance Raman Spectroscopy to Kinetic Studies of Reaction Intermediates[1]

Ling Qin, G. N. R. Tripathi, and Robert H. Schuler*

Radiation Laboratory and Department of Chemistry, University of Notre Dame, Notre Dame, Indiana 46556
(Received: September 19, 1986)

In acidic solution, 1,2,4-benzenetriol is rapidly oxidized by •OH or N_3• to form a mixture of neutral 2,4- and 3,4-dihydroxyphenoxyl radicals. At higher pH these radicals deprotonate (pK_a(1) = 4.75) to form the 2-hydroxy-*p*-benzosemiquinone radical anion which exhibits a prominent resonance Raman band at 1625 cm^{-1} attributable to the Wilson 8a ring stretching mode. In basic solutions this radical subsequently reacts with OH^- to form the radical dianion (pK_a(2) = 8.85) in which the 8a band is shifted to an appreciably lower frequency (1587 cm^{-1}). While the absorption spectra of these latter radicals are very similar and do not allow ready examination of their interconversion by absorption spectrophotometry, the difference between these 8a frequencies is sufficiently great that the Raman method can be used to examine the acid–base equilibrium between the two forms of the radical and to follow the deprotonation kinetics. It is shown that even at high pH the radical monoanion is initially formed on oxidation by N_3• and that deprotonation subsequently occurs by its reaction with base with a rate constant of $(9.6 \pm 1.5) \times 10^9$ M^{-1} s^{-1}. These studies illustrate very well the application of time-resolved resonance Raman spectroscopy as a complement to kinetic spectrophotometry in sorting out the details of secondary processes in pulse radiolysis studies.

To date time-resolved resonance Raman studies of radiolytically produced free radicals have largely been devoted to their qualitative identification and to determination of their spectroscopic properties.[2] Because Raman spectroscopy provides an approach by which one can follow individual components in a reaction mixture it is of interest to use time-resolved Raman methods as a complement to kinetic spectrophotometry in pulse radiolysis experiments, particularly in cases where intermediates have complex and overlapping absorption spectra.[3] In the following we illustrate the potential of this approach with results from a recent study of the oxidation of 1,2,4-benzenetriol (hydroxyhydroquinone) where the singly and doubly charged forms of the semiquinone intermediate present in neutral and basic solutions have very similar absorption spectra, making it virtually impossible to carry out meaningful studies of their interconversion by spectrophotometric methods. However, their Raman spectra are sufficiently different that, as is demonstrated here, this interconversion can be followed readily by time-resolved resonance Raman spec-

(1) The research described herein was supported by the Office of Basic Energy Sciences of the Department of Energy. This is Document No. NDRL-2905 from the Notre Dame Radiation Laboratory.

(2) Wilbrandt, R. *Faraday Discuss. Chem. Soc.* **1984**, 213. Earlier studies on the application of Raman methods in pulse radiolysis studies are summarized.

(3) Tripathi, G. N. R.; Schuler, R. H. *Proceedings of the VI Tihany Conference on Radiation Chemistry*; Budapest, Hungary, in press. Application and limitations of time-resolved resonance Raman methods in radiation chemistry are summarized.

0022-3654/87/2091-1905$01.50/0